JGR Oceans

RESEARCH ARTICLE
10.1029/2018JC014582

A New Definition of the South-East Madagascar Bloom and Analysis of Its Variability

A. F. Dilmahamod[1,2,3,4], P. Penven[2], B. Aguiar-González[3,5], C. J. C. Reason[1], and J. C. Hermes[1,3,6]

[1]Department of Oceanography, University of Cape Town, Cape Town, South Africa, [2]Université Brest, CNRS, IRD, Ifremer, Laboratoire d'Oceanographie Physique et Spatial (LOPS), IUEM, Brest, France, [3]South African Environmental Observation Network, Egagasini Node, Roggebaai, South Africa, [4]Now at GEOMAR Helmholtz Centre for Ocean Research Kiel, Kiel, Germany, [5]School of Marine Science and Policy College of Earth, Ocean and Environment, University of Delaware, Newark, DE, USA, [6]Nelson Mandela University, Port Elizabeth, South Africa

Key Points:
- A revisit of the South-East Madagascar Bloom from updated observations is performed
- Bloom occurs within low-salinity surface waters and coincides with La Nina events as well as reduced coastal upwelling south of Madagascar
- Low-salinity waters, increased stratification, and light provide good conditions for a cyanobacterial phytoplankton bloom

Correspondence to:
A. F. Dilmahamod,
fehmi.dilmahamod@gmail.com

Citation:
Dilmahamod, A. F., Penven, P., Aguiar-González, B., Reason, C. J. C., & Hermes, J. C. (2019). A new definition of the South-East Madagascar Bloom and analysis of its variability. *Journal of Geophysical Research: Oceans*, *124*. https://doi.org/10.1029/2018JC014582

Received 17 SEP 2018
Accepted 16 FEB 2019
Accepted article online 20 FEB 2019

Abstract The South-East Madagascar Bloom occurs in an oligotrophic region of the southwest Indian Ocean. Phase locked to austral summer, this sporadic feature exhibits substantial temporal and spatial variability. Several studies, with different hypotheses, have focused on the initiation mechanism triggering the bloom, but none has been as yet clearly substantiated. With 19 years of ocean color data set available as well as in situ measurements (Argo profiles), the time is ripe to review this feature. The bloom is characterized in a novel manner, and a new bloom index is suggested, yielding 11 bloom years, including 3 major bloom years (1999, 2006, and 2008). Spatially, the bloom varies from a mean structure (22–32°S; 50–70°E) both zonally and meridionally. A colocation analysis of Argo profiles and chlorophyll-a data revealed a bloom occurrence in a shallow-stratified layer, with low-salinity water in the surface layers. Additionally, a quantitative assessment of the previous hypotheses is performed and bloom occurrence is found to coincide with La Niña events and reduced upwelling intensity south of Madagascar. A stronger South-East Madagascar Current during La Niña may support a detachment of the current from the coasts, dampening the upwelling south of Madagascar, and feeding low-salinity waters into the Madagascar Basin, hence increasing stratification. Along with abundance of light, these provide the right conditions for a nitrogen-fixing cyanobacterial phytoplankton bloom onset.

Plain Language Summary The South-East Madagascar Bloom is one of the largest bloom in the world. It can play a major role in the fishing industry, as well as capturing carbon dioxide from the atmosphere. Hence, it needs to be better understood. In previous studies, several hypotheses have been put forward to explain the bloom but none have as yet been clearly substantiated. This study shows that the bloom occurs in a surface layer of low salinity, which tends to favor a specific type of phytoplankton, namely, cyanobacteria. The climate phenomenon, La Niña, also seems to co-occur with the bloom, 10 out of 11 events. The input of nutrient-rich waters to the surface south of Madagascar is weakened during the bloom, and this goes against what was previously thought. The present study gives a possible new reasoning as to why the bloom occurs. The current southeast of Madagascar detaches from the coast and brings low-salinity and nutrient-rich waters into the bloom region where enhanced photosynthesis occurs, hence causing the bloom.

1. Introduction

The region southeast of Madagascar exhibits a major sporadic phytoplankton bloom, the South-East Madagascar Bloom. It was first described as a dendroid bloom, owing to its branching shape (Longhurst, 2001) and represents one of the most dramatic seasonal enhancements in phytoplankton cells in the global ocean. Although phase locked to austral summer/fall (December–April), the bloom exhibits substantial temporal and spatial variability (Srokosz & Quartly, 2013; Uz, 2007; Wilson & Qiu, 2008). It extends over an area of approximately 2,500 km^2 with patches of chlorophyll-a (Chl-a) reaching 2–3 mg/m^3 (Longhurst, 2001) and hence has the potential to play an important role in the biogeochemical cycling of elements (Naik et al., 2015), regulation of atmospheric CO_2 (Lévy et al., 2012), and the oceanic life in the region. To date, the lack of continuous long-term in situ observations and limited model studies have led to a variety of proposed

physical and biological mechanisms behind this phenomenon and, hence, various hypotheses have been suggested to account for the onset of the bloom.

Longhurst (2001) was the first to document the bloom and attributed the onset of the bloom to a mixed layer deepening modulated by the mesoscale eddy field in the region. This would drive nutrients and phytoplankton cells into the euphotic zone through upwelling, with the eddies shaping the surface signature of the subsequent enhanced Chl-a concentration. The following studies also revealed the significance of the highly turbulent circulation in the bloom region, owing to mesoscale eddies, which would disperse nutrients and/or biomass (Huhn et al., 2012; Raj et al., 2010; Srokosz & Quartly, 2013; Srokosz et al., 2004, 2015; Uz, 2007). Srokosz et al. (2004) presented the phytoplankton bloom as the first observed open ocean plankton wave in the Indian Ocean. They hypothesized that a combination of plankton growth and an eastward diffusion owing to the mesoscale circulation, against the mean westward flow, would lead to a plankton wave. However, this eastward displacement can now be attributed to the shallow eastward flow, the South Indian Ocean Countercurrent (SICC; Menezes et al., 2014; Palastanga et al., 2007; Siedler et al., 2006), which has been shown to be present in this region.

Uz (2007) argued that the bloom might be fueled by nitrogen fixation and showed, from Argo floats, that it occurs within a shallow mixed layer depth (MLD) over a strong pycnocline. This process would induce a retainment of nitrogen fixers within the surface layer. The hypothesis proposed involves a higher number of tropical cyclones passing over Madagascar, which would induce enhanced precipitation on the eastern coast of Madagascar, causing increased river runoff (Uz, 2007). These iron-rich waters would be carried alongshore by the South-East Madagascar Current (SEMC) and further advected offshore through eddy-diffusion, fertilizing the region and triggering the bloom. In situ measurements reported by Srokosz and Quartly (2013) confirmed that the bloom is confined to a shallow mixed layer (~30 m), with water temperatures greater than 26.5 °C. Raj et al. (2010) proposed that the interannual variability of the bloom can be supported by the seasonality in precipitation and the current-driven upwelling south of Madagascar. In the same study, the photosynthetically available radiation (PAR) is discussed. With a seasonal maximum in austral summer, it is shown that PAR was at its highest during the bloom years (1999, 2000, 2006, and 2008) compared to non-bloom year (1998) and hence could possibly play an important role in the phytoplankton bloom (Raj et al., 2010).

In situ measurements have shown that in the summer of 2005, the putative nitrogen fixers, namely, *Trichodesmium* and *Rhizosolenia* prevailed in the bloom region (Poulton et al., 2009; Srokosz & Quartly, 2013). The growth of these nitrogen fixers is controlled by various factors such as temperature, light availability (PAR), vertical mixing, competition with other phytoplankton species, and availability of iron and/or phosphorous (Hood et al., 2001, 2004). The populations of *Trichodesmium* and *Rhizosolenia* are mostly found within stable and stratified waters, with temperatures higher than 25 °C (Capone et al., 1997; Subramaniam et al., 2002; Wilson & Qiu, 2008). However, it should be noted that the presence of these species was drawn from a cruise during a year not characterized as a bloom year (Raj et al., 2010; Uz, 2007). Hence, although nitrogen fixers can have an influence on the bloom, as also mentioned by Uz (2007), the possibility of other organisms being predominant during actual bloom years should not be excluded. Sediments on continental shelves, known to be a source of iron in coastal areas (Dale et al., 2015; Jeandel et al., 2011; Johnson et al., 1999), have been proposed as a new origin of iron particles (Srokosz & Quartly, 2013), which would be upwelled to the surface. These particles would be advected eastward, with the bloom ending when all iron particles were depleted. Consistent with Srokosz et al. (2004) and Srokosz and Quartly (2013), Huhn et al. (2012) related this eastward movement to the presence of zonal jets in the SICC and the bloom being shaped by the meridional barrier of these jet-like Lagrangian coherent structures. However, they also concluded that the seasonal and interannual variability of the eastward jets do not match the variability of the bloom.

The strength of the upwelling south of Madagascar may dictate the interannual variability and the size of the bloom, as stated by Lévy et al. (2007), Raj et al. (2010), and Srokosz and Quartly (2013). Contradicting the Longhurst (2001) hypothesis, a shallowing of the mixed layer, which provides good conditions for nitrogen fixers, may also aid in the bloom (Capone et al., 1997; Uz, 2007; Wilson & Qiu, 2008) . Using an eddy-resolving simulation together with a Lagrangian particle tracking, Srokosz et al. (2015) showed that the bloom may be fertilized by iron particles upwelled on the south/southeast of Madagascar and, as suggested by Srokosz

and Quartly (2013), the bloom ends after a depletion of iron particles. Interannual variability of the spatial extent of the Lagrangian particles in this highly turbulent region may explain the spatial distribution of the bloom and that the presence of the SICC is not fundamental to the interannual variability of the bloom (Srokosz et al., 2015). However, using a non-assimilative high-resolution model for the Lagrangian tests, they could not replicate the interannual variability of the phytoplankton cells dispersion, as observed in remotely-sensed data.

With almost 19 years of remotely-sensed ocean color (European Space Agency's Ocean Colour Climate Change Initiative, ESA OC-CCI) data available and long-term in situ measurements (Argo profiles), this study aims to provide a better description of this sporadic bloom. A novel bloom index is suggested from which bloom years are identified, and based on this, an updated temporal and spatial characterization are provided. The existing hypotheses are also reviewed and quantitatively assessed. This paper is structured as follows: the observational data sets and methodology are detailed in section 2; section 3 presents the new bloom index and characterization of the bloom, as well as its associated vertical thermohaline structure; section 4 revisits existing hypotheses, and lastly, section 5 summarizes the results.

2. Data and Methods

2.1. Data to Characterize the South-East Madagascar Bloom

The version 3 chlorophyll-a concentration product, provided by the ESA OC-CCI (www.esa-oceancolour-cci.org; Lavender et al., 2015; Satyendranath et al., 2016) was used in this study. It combines data from Sea-viewing Wide Field-of-view Sensor (SeaWiFS), MEdium Resolution Imaging Spectrometer, and MOderate Resolution Imaging Spectroradiometer-Aqua (MODIS) to provide a continuous time series of surface chlorophyll-a concentration from September 1997 to December 2016. At a spatial resolution of $\frac{1}{24}°$ (~4.5 km), 8-day composites from January 1998 to December 2016 (19 years) were acquired so as to maximize coverage. In addition, data at this temporal resolution are sufficient to properly capture the temporal structure of the bloom.

The PHYSAT algorithm was developed to identify dominant phytoplankton groups simultaneously with Chl-a, using the daily global SeaWiFS data set (Alvain et al., 2005). Available as monthly averages from 1997 to 2010, with a spatial resolution of 9 km, this method detects the major dominant phytoplankton groups namely nanoeucaryotes, Prochlorococcus, Synechococcus, diatoms, phaeocystis, and coccolithophorids. This is performed by identifying specific signatures in the water-leaving radiances spectra measured by ocean color satellites. The process is described in detail by Alvain et al. (2005).

The international Argo program (Argo, 2000) consists of a global array of ~3,800 free-drifting profiling floats. These Lagrangian robots provide freely available data of temperature and salinity down to 2,000 m every 10 days (Coriolis Project: http://coriolis.eu.org). In the Indian Ocean, these vertical profiles of temperature and salinity are available from 1999 to 2016. Automatic pre-processing and quality control measures are performed by the Argo Data Centre (Böhme & Send, 2005; Owens & Wong, 2009; Wong et al., 2003). Two additional criteria, based on the quality control flags and sampling characteristics, are applied to retain only good data: (1) Only temperature, salinity and pressure data flagged 1 (good) and 2 (potentially good) were considered; (2) Only profiles with at least four data points in the first 50 m, with the shallowest data point being between the surface and 20 m, are examined.

The optimal interpolation "In Situ Analysis System (ISAS)" provides gridded fields of salinity from the surface ocean to 2000 m deep, on $\frac{1}{8}°$ spatial resolution (Gaillard et al., 2016; Kolodziejczyk et al., 2017). This product is based entirely on in situ measurements namely the ARGO network, TAO-TRITON moorings, and CTD casts. Monthly fields of version 7 of the ISAS data are used in this paper.

2.2. Data and Methods to Test the Different Hypotheses

Since it was first documented by Longhurst (2001), different hypotheses have been suggested to explain the mechanisms responsible for the onset of the South-East Madagascar Bloom. Using longer available data sets, a quantitative assessment of each hypothesis is performed. This involves a predictive skills assessment of time series of the physical variable related to a specific hypothesis. Hereafter referred as a "quantitative hypothesis testing," this provides an indication of a possible validity of the specific hypothesis, based on different time lags and variable thresholds.

The quantitative hypothesis testing is conducted as follows: (1) From 1998 to 2016, each year is described as either a year of bloom or nonbloom occurrence, based on a specific criterion (see bloom and nonbloom identification in section 3.1). (2) During a bloom year, the month of interest is ascribed to the month during which the austral summer bloom is at its maximum. Since the bloom does not always peak during the same month (section 3.2), for a nonbloom year, the nonbloom month of interest is set to January, February, March, or April. (3) The physical variable associated with the specific hypothesis is tested against the bloom and nonbloom months at 0, 1-month, 2-month, and 3-month lags. (4) For each lag, values of the physical variable, specific to the hypothesis, which coincide with the bloom and nonbloom months are assigned. (5) These values are then compared against different thresholds. From this, a success rate is calculated. This is done by considering the total number of bloom and nonbloom years being able to be predicted by the threshold. For example, if nine bloom and three nonbloom events over 19 years of Chl-a data set are correctly predicted, this will result in a 63% ((9 + 3)/19) success rate. (6) Hence, the threshold of a specific lag, which yields the maximum success rate by correctly predicting the most number of bloom and nonbloom years over the 19-year data set, is retained and termed as an "optimized threshold and lag." The relationship of the different physical/biogeochemical variables and their corresponding hypothesis are detailed below.

Longhurst (2001) ascribed the bloom to a seasonal deepening of the MLD, modulated by the mesoscale eddy field in the region. To evaluate this hypothesis, a mixed layer data set based on a new Argo gridded data set (Barnes objective analysis, BOA-Argo) version 7 (Li, Liu, et al., 2017; Li, Xu, et al.,2017) is employed. The geometry method described by Chu et al. (1999) is used to calculate the MLD for each Argo profile. These monthly MLD data are available from January 2004 to December 2017, on a 1° × 1° grid.

Srokosz et al. (2004) described the South-East Madagascar Bloom as the first observed open ocean plankton wave. They described the bloom as having a rapid eastward spread, with a combination of plankton growth and eddy diffusivity playing a role. A turbulent eddy diffusivity parameter (A_H) is obtained from satellite altimetric observations of Eddy Kinetic Energy (EKE). The EKE is derived from daily geostrophic current data, with mean dynamic topography produced by SSALTO/DUACS and distributed by the Archiving, Validation and Interpretation of Satellite Oceanographic (AVISO) data, on a 0.25° grid.

Following Sallée et al. (2008), an eddy diffusivity coefficient can be inferred as

$$A_H = \alpha \times \sqrt{EKE} \times L_d \tag{1}$$

where L_d is the baroclinic Rossby radius of deformation; the square root of the EKE, $\sqrt{EKE}$, yielding the eddy velocity, and the coefficient α is set to 1.35. This value holds in energetic areas with EKE higher than 0.015 m^2/s^2 (Sallée et al., 2008). High EKE is observed southeast of Madagascar, and hence, this specific α may be used in this study.

Uz (2007) proposed that an increase in precipitation, owing to tropical cyclones, will induce enhanced river runoff of iron-rich sediments into the open ocean and ultimately causing a bloom. Hence, the global oceanic and land precipitation, obtained from the Climate Prediction Center Merged Analysis of Precipitation (Xie & Arkin, 1997), is examined in the 47.5–52.5°E; 12.5–25°S region, consistent with Uz (2007). This data set combines gauge station measurements as well as satellite-derived precipitations and consists of a global 5-day (pentad) estimate, produced on a 2.5° latitude-longitude grid and spanning from 1979 to the present.

Uz (2007) and Raj et al. (2010) stated that Ekman pumping (W_{ek}) southeast of Madagascar is too small to have any influence on the bloom. Nevertheless, this region is prone to tropical cyclones in austral summer, and these climatic events are known to largely influence the W_{ek} and eventually the primary production (Chacko, 2017; Lin et al., 2003). The influence of surface wind stress is assessed using the European Centre for Medium range Weather Forecasting (ECMWF) Re-Analysis (ERA-Interim) wind product (Dee et al., 2011). It is a global climate reanalysis from 1979 to date and is updated in near real time. Produced using a data assimilation system, it has a 0.75° × 0.75° spatial resolution and a daily temporal resolution. W_{ek} is calculated as

$$W_{ek} = \frac{1}{\rho_w f} curl\tau \tag{2}$$

where ρ_w is the density of sea water (1,025 kg/m^3), f is the Coriolis parameter, and τ is the wind stress component.

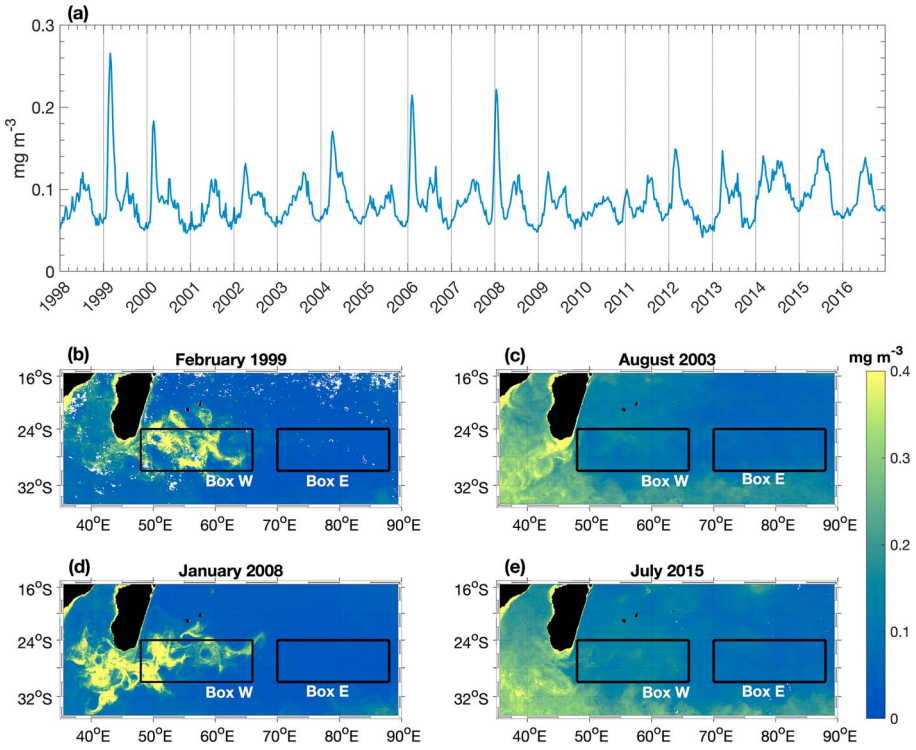

Figure 1. (a) Time series of ESA OC-CCI mean Chl-a concentration (mg/m^3) in the bloom box (box W), as defined by Uz (2007), from 1998 to 2016. Two specific events of austral summer blooms in February 1999 (b) and January 2008 (d), and austral winter blooms in August 2003 (c) and July 2015 (e). The overlaid boxes in (b)–(e) delineate the "bloom box" (box W) and the similarly sized box offshore (box E).

Raj et al. (2010) also stated the importance of light availability in supporting the phytoplankton bloom. Based on this, monthly composites data set of PAR data are retrieved from SeaWiFS at a 9-km spatial resolution (1997–2010) and MODIS at 4-km spatial resolution (2003–2016; from http://oceancolor.gsfc.nasa.gov).

In several studies, the current-driven upwelling south of Madagascar has been hypothesized to be the main mechanism that contributes to the bloom and which controls its interannual variability (Lévy et al., 2007; Raj et al., 2010; Srokosz & Quartly, 2013; Srokosz et al., 2015). Two coastal upwelling indices are used to study this relationship. The first one is a sea surface temperature (SST)-based coastal upwelling index (CUI; Ramanantsoa et al., 2018), which reports the influence of the SEMC on the coastal upwelling south of Madagascar. An optimum interpolated high-resolution SST, provided by the Advanced Very High Resolution Radiometer infrared satellite data, is used. These are obtained at a daily temporal resolution and on a 0.25° grid. The second index is based on Chl-a concentration anomalies, which is used as a proxy of upwelling since nutrient-rich waters being brought to the surface indicates an increase in phytoplankton cell concentration. Accordingly, the Chl-a concentration comprising the two upwelling cores south of Madagascar (Ramanantsoa et al., 2018; 44–47.5°E; 25–25.8°S), both inshore of the SEMC, was considered. This is inferred from the Chl-a data set of ESA OC-CCI.

3. Description of the South-East Madagascar Bloom

The region southeast of Madagascar exhibits both an austral summer and winter bloom (Figure 1a). However, while the summer bloom does not occur every year, it can be up to 2 or 3 times stronger than the winter bloom. The latter is a more recurrent and regular phenomenon of the Chl-a phenology. Uz (2007) described the South-East Madagascar Bloom using a box (24–30°S; 48–66°E), termed as the "bloom box" (box W in Figures 1b–1e). Two events of maximum phytoplankton bloom, in both austral (February 1999 and January 2008) and winter (August 2003 and July 2005) are identified and shown in Figures 1b–1e. The spatial contrast between the two seasonal blooms is evident. The South-East Madagascar Bloom displays a branching

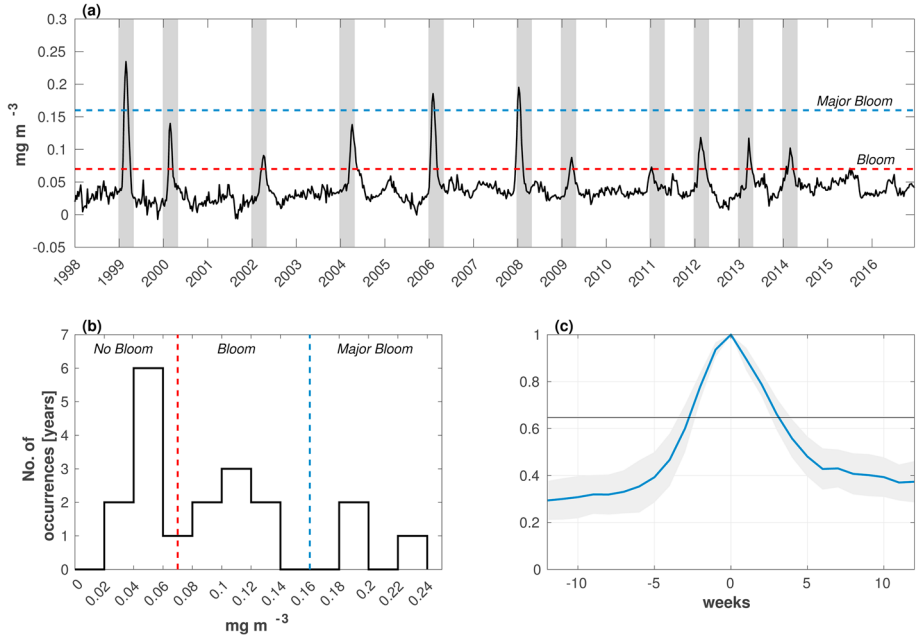

Figure 2. (a) Bloom index computed by subtracting Chl-a of box E from "bloom box" (box W), identified in Figures 1b–1e. (b) Histogram of the maximum yearly difference in Chl-a concentration (mg/m^3) between bloom box and box E. Panel (c) displays a mean temporal composite of the bloom. In both (a) and (b), the red dotted line indicates the threshold of 0.07 mg/m^3, which distinguish the bloom and nonbloom years. The blue dotted line indicates the 0.16 mg/m^3 threshold, which separate major bloom from normal bloom years. In (a) and corresponding later figures, the gray shading indicates the bloom years.

shape, with spots of high Chl-a patches. On the other hand, the winter bloom exhibits a more evenly spread Chl-a concentration, with some patches of enhanced Chl-a.

In this section, the main features of the South-East Madagascar Bloom are revisited. Using a 19-year (1998–2016) ocean color data set, the bloom is characterized and its associated temporal and spatial variabilities are detailed. Based on this longer data set, a more comprehensive view of the bloom than previously achieved can be given.

3.1. Identification of Bloom/Nonbloom Years

To unveil the timing of the bloom, Uz (2007) normalized the Chl-a concentration in the bloom box by a similarly sized box (box E: 24–30°S; 70–88°E) located to the east, toward the open ocean (box E in Figures 1b – 1e). However, this normalization can be deceptive since it provides no information on the intensity of the austral summer bloom, as the peaks would be highly dependent on the winter bloom in box E, for which the values are close to 0. On this basis, the "bloom index" is redefined in this study, by subtracting the Chl-a concentration of box E from the bloom box (box W), hence providing an improved diagnosis of the timing as well as the intensity of the bloom (Figure 2a).

A threshold criterion can be used to quantify a bloom frequency and trend (Tett, 1987). To define the threshold, a histogram is built from a yearly maximum of Chl-a difference (bloom box- box E), computed from January to April, owing to an austral summer occurrence of the bloom. The first exceedance of a specific Chl-a concentration difference threshold is applied to distinguish between occurrence of bloom and nonbloom years. A trough is observed in the maximum Chl-a difference occurrences, at 0.07 mg/m^3, a threshold that would be used to differentiate bloom years from nonbloom years (Figure 2b). However, no events of maximum Chl-a difference occurred between 0.14 and 0.18 mg/m^3 beyond which, three more events took place. Hence, accordingly, a 0.16 mg/m^3 exceedance threshold is assigned to separate normal from major bloom events. Respectively, these account for eight and three events.

3.2. Temporal Variability

From the new redefined bloom index, 11 bloom years are identified, namely, 1999, 2000, 2002, 2004, 2006, 2008, 2009, 2011, 2012, 2013, and 2014. It should be noted that these fully agree with Uz (2007), who also

Table 1
Events of Bloom and Nonbloom Years, With Bloom Years Being Defined as Normal and Major Blooms

	Bloom			
Years	Bloom (0.07–0.16 mg/m^3)	Major bloom (>0.16 mg/m^3)	Month of maximum bloom	Nonbloom
1998				X
1999		X	February	
2000	X		March	
2001				X
2002	X		April	
2003				X
2004	X		April	
2005				X
2006		X	February	
2007				X
2008		X	January	
2009	X		March	
2010				X
2011	X		January	
2012	X		March	
2013	X		April	
2014	X		March	
2015				X
2016				X

Note. The month during which the bloom is maximum is stated in the fourth column. Bloom years are listed in bold.

classified 1999, 2000, 2002, and 2004 as bloom years. However, as seen in Figure 2a, the intensity of the bloom exhibits substantial variability, with the most prominent blooms occurring in 1999, 2006, and 2008 (>0.16 mg/m^3; major blooms), while normal blooms occur during the remaining bloom years. These are summarized in Table 1.

Another interesting feature of the bloom is that, although it is phase locked to austral summer, it does not always initiate or peak during the same month (Figure 2a). Typically, the bloom commences in January, peaking in February and diffusing by March/April. However, variations are observed from one event to the next. During the three strongest events, the phytoplankton bloom peaked in January (2008) and February (1999 and 2006). In 2008, the bloom started at the end of the previous year (2007), whereas for 1999 and 2006, it started in January (Figure 2a). In other bloom years, the initiation month is delayed, starting in February (2002 and 2004), and peaking later in April. In 2012, 2013, and 2014, the bloom reaches its highest intensity around the end of March. The mean duration of the bloom is observed from a temporal composite to be ~6 weeks (Figure 2c), with the feature developing quicker than it dissipates (also observed during the bloom peaks in Figure 2a).

3.3. Mean Spatial Structure and Variability of the Bloom

In addition to the large temporal variability exhibited by the bloom, its spatial extent also varies significantly both meridionally and zonally. Months of maximum Chl-a concentration during identified bloom years, as well as Januarys of nonbloom years, are used to construct a composite Chl-a map of bloom (Figure 3a) and nonbloom (Figure 3b) periods. This reveals a mean spatial structure of the bloom, with enhanced Chl-a observed around the southern part of Madagascar, and the bloom identified as an elongated filamentous structure on its southeastern flank, extending eastward well out into the open ocean. The 0.07 mg/m^3 provides a compelling view of the zonal extent of bloom period, compared to nonbloom period (Figure 3). From this mean structure, a Chl-a concentration of around 0.25 mg/m^3 in the Madagascar Basin and south of Madagascar can be observed, with patches of lower concentration on the peripheries of the bloom. The mean structure of the feature varies meridionally from 22°S to 32°S and zonally from 50°E to ~70°E (Figure 3a),

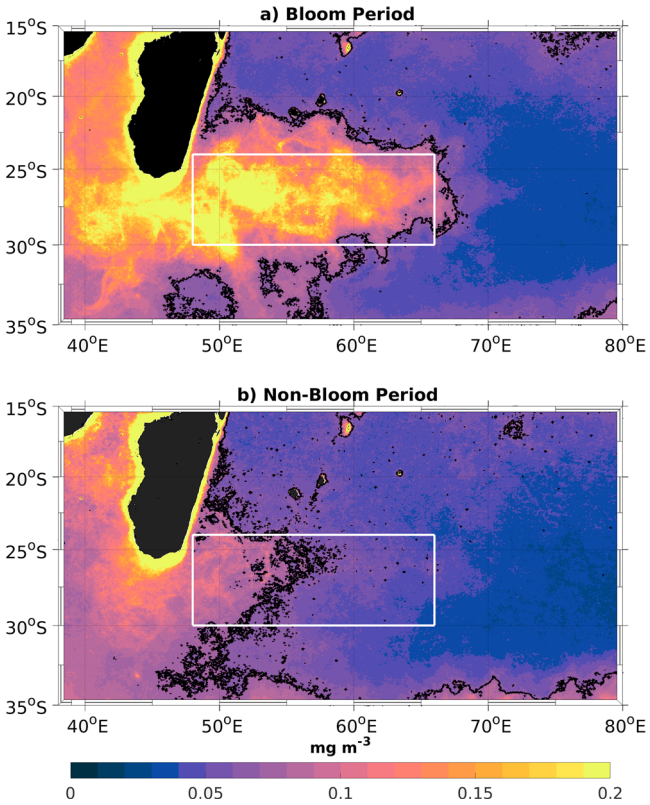

Figure 3. (a) Spatial maps of mean ESA OC-CCI Chl-a concentration (mg/m^3) during months of maximum austral summer bloom identified in Figure 2a. (b) Same as (a) but during January of minimum Chl-a concentration in austral summer. The black contour denotes the 0.07 mg/m^3 threshold used to distinguish between bloom and non-bloom years.

hence covering a surface area of ~2,600,000 km^2. Interestingly, during nonbloom periods, a filamentous structure exists close to the coast with some slight patches of enhanced Chl-a, which however does not extend as far east as in the bloom period (Figure 3b).

As previously mentioned, the bloom reaches its highest intensity at different months of austral summer and displays strong spatial variability. Figure 4 shows the Chl-a distribution for the month which exhibits maximum concentration in the bloom box, for each year from 1998 to 2016. The zonal and meridional extents, as well as the enhanced Chl-a on the southwestern and southern parts of the Madagascan coasts, vary from one bloom year to the next (Figure 4). A first glimpse from this figure reveals the presence of some patches of higher Chl-a concentration, during almost every year in the bloom box, except during the identified "bloom years," when the enhanced Chl-a patches are exceptional.

A compelling component of the bloom is its connection to the Madagascan coast (Figure 4). During some bloom years, enhanced Chl-a signatures appear linked to the southeastern and/or southern coast of Madagascar (1999, 2000, 2002, 2006, 2008, and 2012), whereas during other bloom years (2004, 2009, 2013, and 2014), the bloom seems disconnected from the coast by a low Chl-a region. These differences can possibly be associated with a different triggering mechanism between the offshore and coastally-linked blooms. In some nonbloom years, traces of weak Chl-a concentration also develop in the Madagascar Basin (2003, 2005, 2010, 2015, and 2016; Figure 4). The longitudinal extent of the bloom, when fully developed, can reach up to 72°E (1999, 2006, and 2008). However, in other years, it can extend only to about 60–65°E. The latitudinal band at which the bloom prevails varies from one bloom year to another, with the strongest blooms (1999, 2006, and 2008) appearing mostly in the 22–30°S band. Comparatively, the 2012 bloom is shifted southward (25–34°S).

On a biological note, the dominant phytoplankton groups, from PHYSAT, prevailing in the bloom box is investigated (not shown here) during months of maximum bloom in 1999, 2000, 2002, 2004, 2006, 2008,

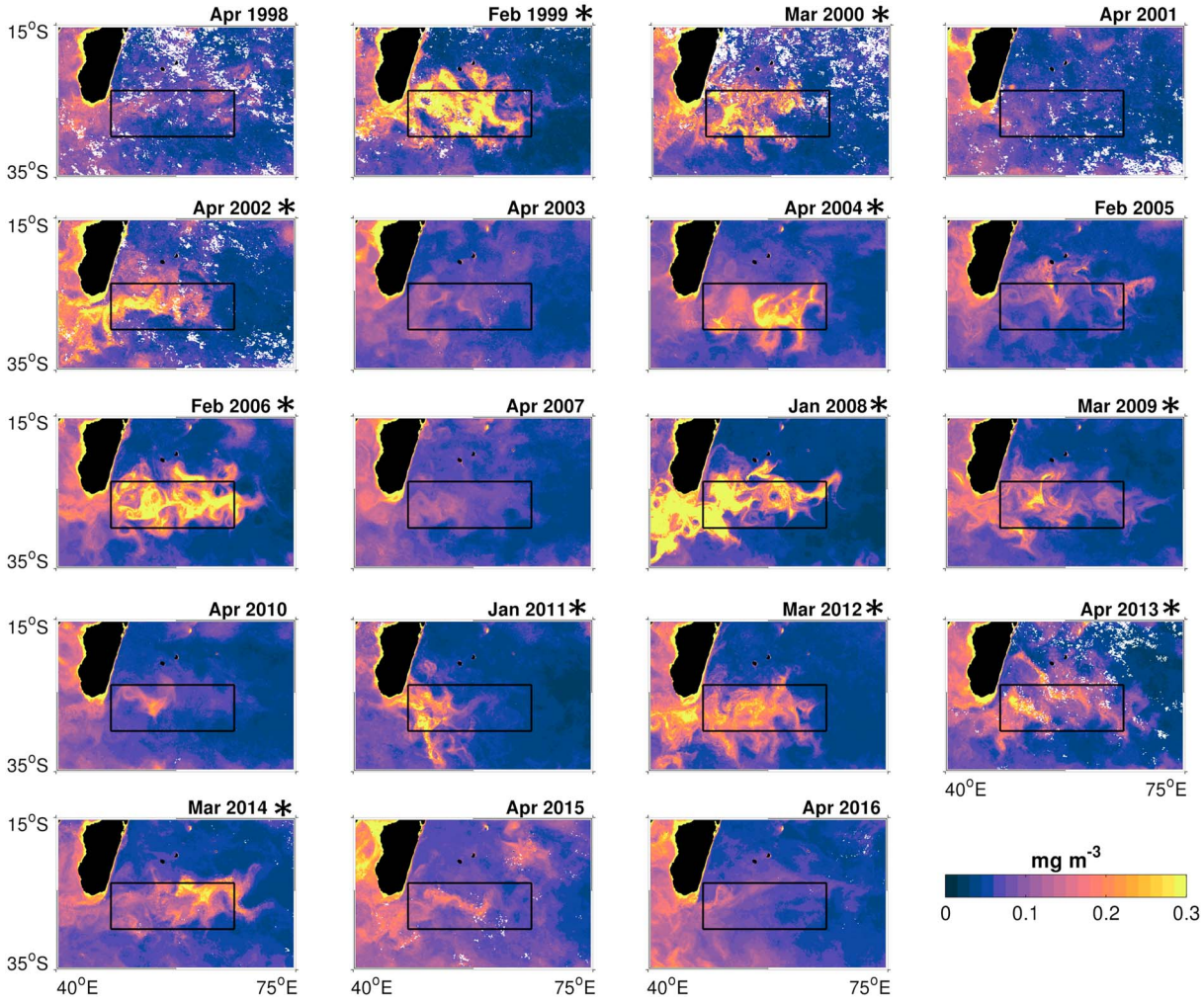

Figure 4. Spatial maps of the months of maximum ESA OC-CCI Chl-a concentration (mg/m^3) observed in "bloom box," from 1998 to 2016. The asterisk denotes years identified as bloom years from Figure 2a.

and 2009. However, February 2008 is considered instead of January 2008, owing to a gap in the January data set. On average, the South-East Madagascar Bloom box is dominated by the following phytoplankton group (number of pixels ± standard deviation): Prochloroccocus (1,105 ± 226), Synechococcus (993 ± 434), nanoeucaryotes (206 ± 128), phaeocystis (38 ± 20), and diatoms (31 ± 41). Prochloroccocus and Synechococcus from the phylum cyanobacteria prevailed in the bloom region.

3.4. Vertical Structure

Co-located Argo profiles and high/low Chl-a patches are used to investigate the mean structure of the water column in the bloom domain. A threshold of Chl-a concentration greater (less) than 0.27 (0.06) mg/m^3 is used to identify which float is in a bloom (nonbloom) area. These thresholds were chosen to capture patches with high and low Chl-a contents, respectively, and to have an adequate number of Argo profiles in both cases. It should be noted that a surface salinity front, assumed to be associated with the SICC (Menezes et al., 2014; Siedler et al., 2006), is present in the region, with lower salinity equatorward and higher salinity poleward. This front varies latitudinally throughout the year but does not deviate significantly during months of maximum bloom years. To prevent any bias in the mean haline vertical structure of bloom and nonbloom spots, an isohaline of 35.4 psu (green line in Figures 5a and 5b) is used as a threshold to separate the fresher (less saline) and saltier (more saline) sides of this front. This separation of Argo profiles in Chl-a patches will provide a mean water column structure on the two sides of the front. Henceforth, Argo profiles in high Chl-a patches are referred to as "bloom profiles," and profiles in low Chl-a as "nonbloom profiles."

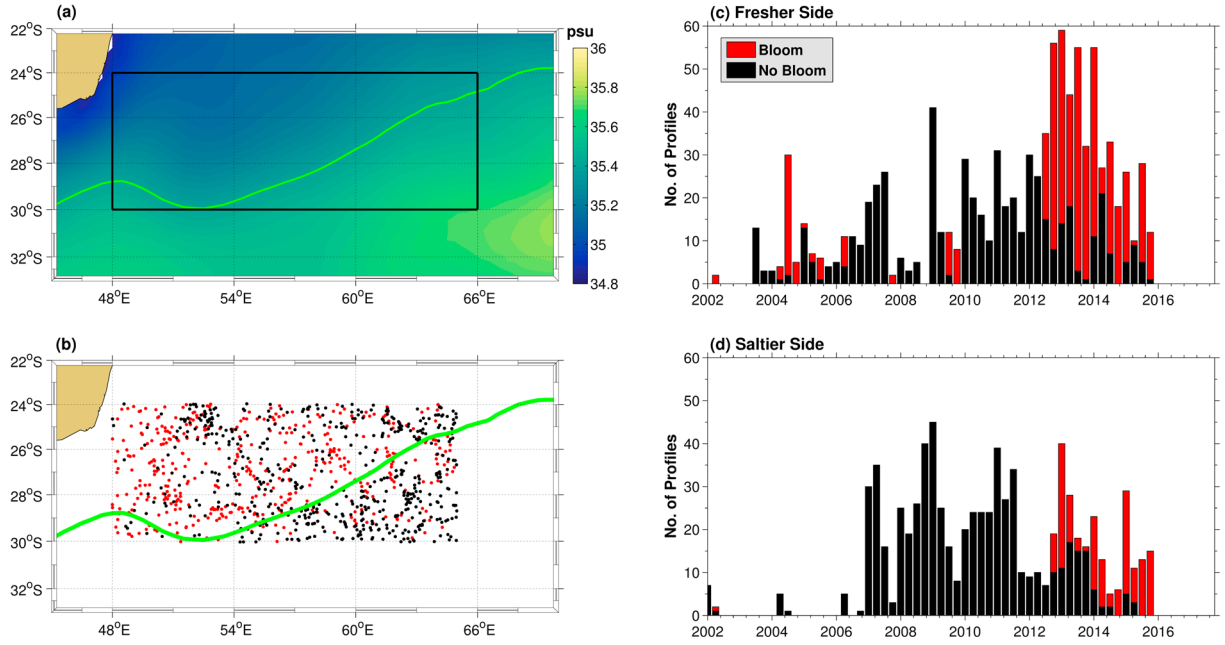

Figure 5. (a) Mean ISAS sea surface salinity (psu), averaged during January–April over the 2002–2015 period, with the green contour delineating the 35.4-psu isohaline. Panel (b) indicates the positions of bloom (red) and nonbloom (black) profiles in the bloom box, separated by the 35.4-psu isohaline (green line). Panels (c) and (d) display the number of bloom (red) and nonbloom (black) profiles surveyed in each austral summer months (January–April), from 2002 to 2015, for the fresher (equatorward) and saltier (poleward) sides of the isohaline respectively.

The 731 (291) bloom profiles and 540 (622) nonbloom profiles were obtained on the fresher (saltier) side of the front, and these were spatially well distributed over the bloom box (Figure 5b). A higher number of bloom profiles surveyed are expected in bloom years and vice versa (Figures 5b–d). However, this remains arbitrary as the number of profiles in the ocean have increased since the first Argo float deployment. On the fresher side of the salinity front, nonbloom years of 2005, 2007, and 2010 were mostly surveyed. In 2009, even though a bloom occurs, nonbloom profiles were more abundant, possibly due to the broader distribution of the high Chl-a patches during this year (2009 in Figure 4). Frequent profiling occurred in 2012, 2013, and 2014, years, which have been identified as bloom years (Figure 2a and Table 1). On the saltier side of the front, nonbloom profiles were more abundant. This could either mean that the bloom occurs more frequently on the fresher side of the salinity front or that more Argo profiles were present on the higher salinity side of the front during the phytoplankton bloom. However, the number of profiles in high Chl-a patches were higher toward the end 2012, early 2013, and early 2014 (bloom years). The higher number in April 2012 could be due to the southward migration of the bloom during that year (Figure 4).

The mean surface temperature in both bloom and nonbloom areas is about 26.2–26.5 °C (fresher side; Figure 6a), and 24.8 °C (saltier side; Figure 6c). On the fresher side, the slightly lower surface and subsurface temperatures associated to the bloom profiles could be representative of upwelling. The depths of the mixed layer associated with bloom and nonbloom patches are quite similar (~23.6 m) on the fresher side of the bloom. On the more saline side, nonbloom profiles exhibit a shallower MLD (~19 m) compared to bloom profiles (~23.1 m). Overall, in the bloom box, the mixed layer associated with the bloom remains shallow. The compelling signature in the associated bloom/nonbloom mean thermohaline structures is that the bloom is confined to a surface layer exhibiting a lower salinity signature compared to the nonbloom profiles, on both sides of the front (Figures 6b and 6d).

The mean vertical structures of the water column, associated to high and low Chl-a patches during the bloom event of January 2008 (Figure 7a) and March 2012 (Figure 7d) are investigated using individual profiles of Argo floats. Two bloom profiles (denoted as 1 and 2) and two nonbloom profiles (denoted as 3 and 4) are considered and surveyed. The 2008 bloom is confined to a shallow (~20.4 m) stratified MLD (Figure 7b). However, the vertical haline structure of the two bloom profiles varies, with profile 1 exhibiting higher salinity (~35.5 psu) in the first 20 m compared to profile 2 (~35.1 psu; Figure 7c). Compared to profile 1, profile 2 is located more equatorward and hence possibly on the fresher side of the front. It is also located on the

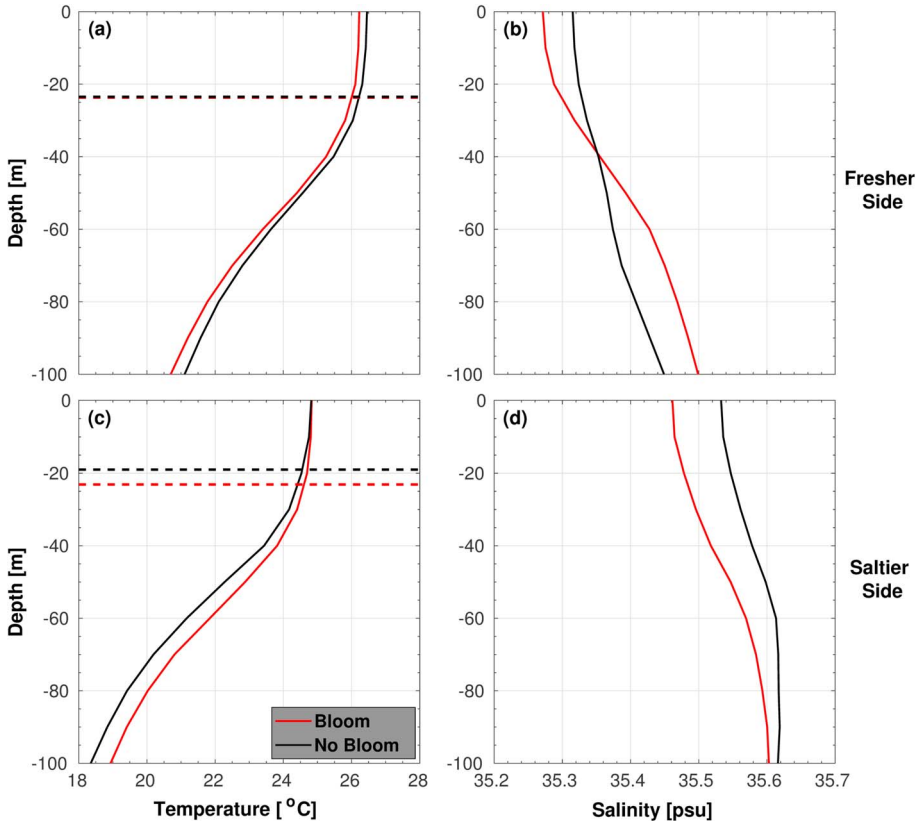

Figure 6. The mean vertical thermohaline structure of the water column associated with bloom (red line) and nonbloom (black line) years on the fresher side (upper panels) and saltier side (lower panels) of the salinity front. The red and black dotted lines show the mixed layer depth of the bloom and nonbloom areas, respectively.

peripheries of a cyclonic eddy situated close to the Madagascan coast, which could be advecting low-salinity SEMC waters away from the coast (Figure 7a). Profile 1 exhibits a salinity signature (Figure 7c) quite close to the mean salinity of bloom profiles on the saltier side of the front (Figure 6d). For nonbloom profiles (3 and 4), a deeper mixed layer (26.3 m for profile 3 and 40.9 m for profile 4; Figure 7b) is observed, associated with a higher salinity in the surface layers, compared to bloom profiles (Figure 7c).

During the bloom event of March 2012 (Figure 7d), profile 1 is confined within a shallow-stratified mixed layer (~24.1 m), whereas profile 2 occurs within a deeper mixed layer (~31.7 m; Figure 7e). As in January 2008, nonbloom profiles are found to be associated with a deeper mixed layer (Figure 7e), except profile 3, which exhibits a MLD of 26.3 m (Figure 7e). In regard to the associated thermohaline structures, no big difference is observed in the salinities between bloom and nonbloom profiles. The bloom profiles (1 and 2) have similar salinity signatures (~35.4 psu; Figure 7f), with profile 1 having a slightly lower surface salinity. The salinity of profile 2 remains quite stable down to ~75 m deep, whereas for profile 1, it increases by ~0.2 psu, from 20 to 40 m.

4. Quantitative Hypothesis Testing

In this section, the various hypotheses proposed in earlier studies are examined. The time series of Chl-a concentration in the bloom region is discontinuous, and hence, a continuous correlation between the bloom and the different variables associated with specific hypotheses cannot be performed. On this basis, a quantitative hypothesis testing method is employed (see section 2.2). This analysis is performed using detrended time series of the specific variable associated with each hypothesis, owing to the presence of a trend in some cases. Figures 8 and 9 display a combination of outputs from the quantitative hypothesis testing. In each figure, the green dotted line indicates the optimized threshold which yields the maximum success rate. The red (blue) dot designates the month when the specific hypothesis holds true for a bloom (nonbloom) year, whereas the pink cross shows the inability of the hypothesis to explain a bloom or nonbloom. If as a null

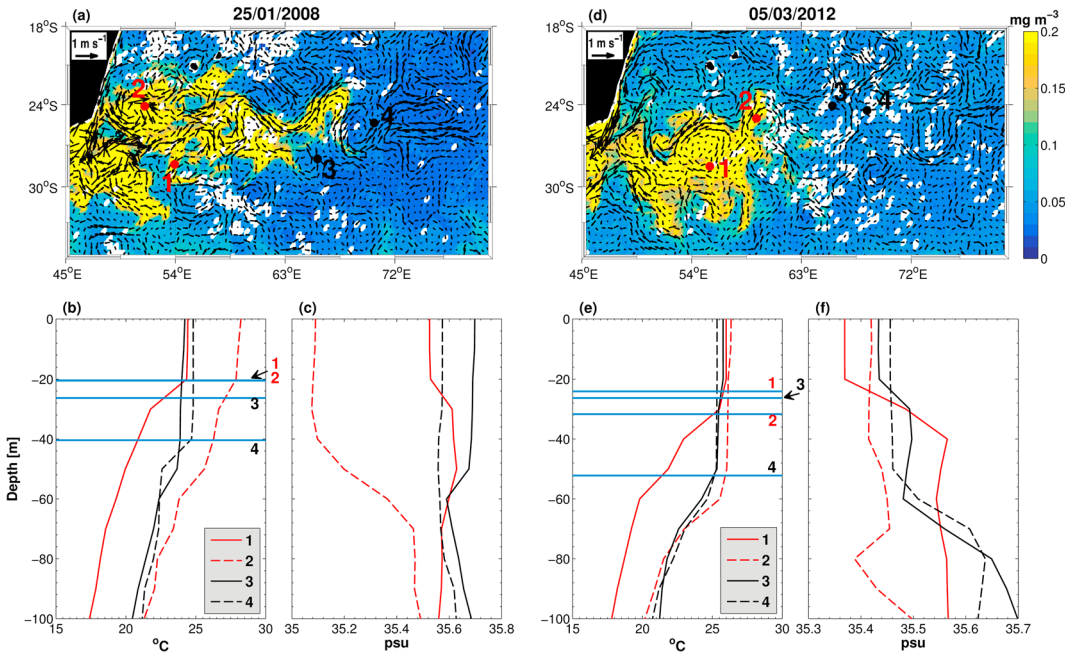

Figure 7. Snapshots of two bloom events, (a) 25 January 2008 and (d) 5 March 2012, with positions of four Argo profiling floats. Floats 1 and 2 are located in an enhanced Chl-a region (bloom), whereas Floats 3 and 4 are found in low Chl-a patches (nonbloom). The bottom panels give the vertical structure of these eight floats' locations. The assigned blue lines display the mixed layer depth from each profile.

hypothesis, we state that all years (1998–2016) are bloom years, on the basis of 11 identified bloom years, this will result in a success rate of 58%. Hence, a hypothesis giving a maximum success rate close or less than 58% should not be regarded as the main mechanisms at play.

4.1. MLD (Longhurst, 2001)

The quantitative hypothesis testing returned a success rate of 69%, with a threshold of 0 m for the MLD anomaly, at a 0-month lag. It should be noted that the success rate was calculated over the 2004–2016 time frame, owing to paucity of in situ data before 2004. In some of the years during which the bloom occurred, the mixed layer became shallower (2004, 2006, 2008, 2011, 2012, and 2014; red dots in Figure 8a). Years 2007, 2015, and 2016 exhibited deeper mixed layers (Figure 8a), hence consistent with no bloom during these years.

4.2. Plankton Wave (Srokosz et al., 2004)

An increasing trend was noticed in the EKE, in agreement with Backeberg et al. (2012), as well as the eddy diffusivity (A_H), southeast of Madagascar. Accordingly, the data set was detrended by its mean value, before applying the hypothesis testing method. An enhanced eddy diffusivity would favor the plankton wave hypothesis, by transporting upwelled nutrients and subsequently growing plankton eastward. On the other hand, lower values of A_H would follow a nonbloom occurrence. A 68% success rate was obtained when the A_H for bloom (nonbloom) months exceeded (did not exceed) a threshold of 0- at a 1-month lag (Figure 8b). A_H in 1999, 2000, 2002, 2004, 2006, 2008, and 2011 (red unit in Figure 8b) exceeded the optimized threshold and this could possibly contribute to the phytoplankton bloom. Lower diffusivity was observed in 1998, 2001, 2005, 2010, 2015, and 2016 (Figure 8b), in accordance to these being no-bloom years.

4.3. Iron Runoff (Uz, 2007)

The relationship between precipitation and occurrence/non-occurrence of the phytoplankton bloom was expected to occur within a certain lag, owing to the time taken for the iron particles from land to be washed into the ocean, transported southwards by the SEMC and ultimately ending in the bloom vicinity. Through a Lagrangian analysis, a 1- to 4-months laps of time was observed as the time taken for particles to propagate from the southeast Madagascar coast to the bloom region (see Figure 6 in Srokosz et al., 2015). The quantitative hypothesis testing yielded a maximum success rate (53%) with a threshold of 1.66 mm/day, at a 1-month lag. This success rate, however, included mostly the years of nonbloom occurrence (1998, 2001,

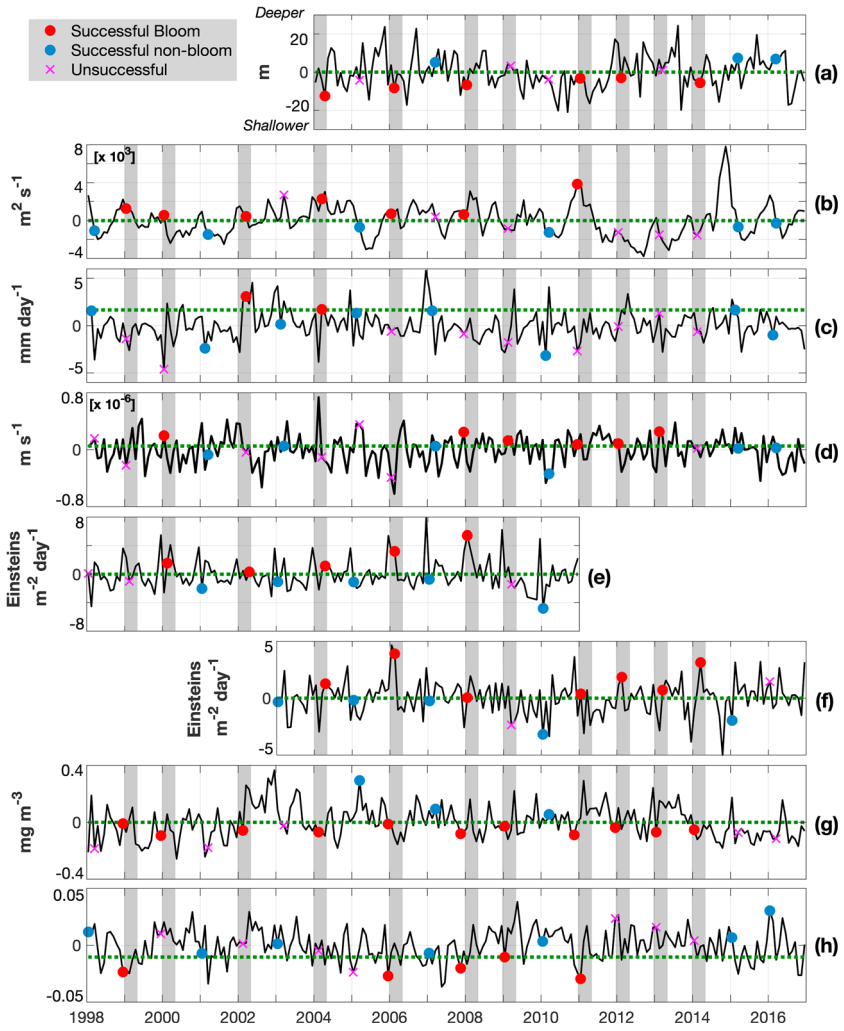

Figure 8. Monthly time series of detrended (a) mixed layer depth anomalies, (b) eddy diffusivity, (c) precipitation anomalies, (d) Ekman velocity, (e) PAR-SeaWiFS anomalies, (f) PAR-MODIS anomalies, (g) Chl-a-based upwelling index based on Chl-a anomalies close to the southern Madagascan coast (44–47.5°E; 25–25.8°S), and (h) SST-based upwelling index anomalies. The gray shading shows bloom years. The green dotted line displays the optimized threshold, which yields the maximum success rate, with the red and blue dots designating the month when the hypothesis holds true for bloom and nonbloom year, respectively. The pink cross indicates the year when the hypothesis does not work.

2003, 2005, 2007, 2010, 2015, and 2016) compared to the bloom occurrence ones (2002 and 2004; Figure 8c). The other years identified as bloom years do not seem to occur during high rainfall which would cause excess river runoff.

4.4. Ekman Pumping (Raj et al., 2010; Uz, 2007)

In the bloom region southeast of Madagascar, positive W_{ek} prevailed during austral summer compared to austral winter (not shown here). Although higher frequency winds could have an important impact on the bloom, the quantitative hypothesis testing was applied on detrended monthly means of W_{ek} (Figure 8d), as a monthly integrated view is of interest here. An W_{ek} threshold greater than 0.06×10^{-6} m/s for bloom and nonbloom occurrence at a 1-month lag yielded a 63% success rate. Six years were correctly hypothesized by the optimized threshold, in regard to bloom (2000, 2008, 2009, 2011, 2012, and 2013) and nonbloom (2001, 2003, 2007, 2010, 2015, and 2016) occurrences. The main significant signal is the highly positive W_{ek} in 2004 (Figure 8d), which might possibly play a major role in the 2004 bloom. Nonetheless, the quantitative hypothesis testing did not account for this specific signal since it occurred in February, 2 months before the peak (April) of the 2004 bloom.

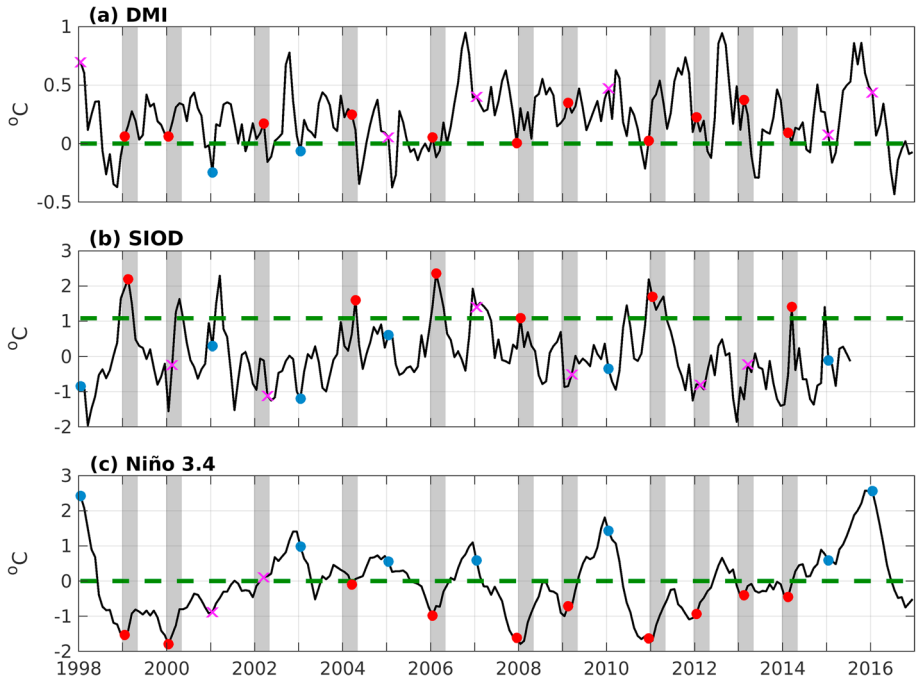

Figure 9. Same as *Figure* but for (a) Dipole Model Index (DMI), (b) Subtropical Indian Ocean Dipole (SIOD), and (c) Niño 3.4.

4.5. Light Availability (Raj et al., 2010)

The quantitative hypothesis testing yielded a success rate of 86% (SeaWiFS) and 74% (MODIS) for PAR anomalies, with an optimized threshold of 0 Einstein·m^{-2}·day^{-1} at 0-month lag for a bloom and nonbloom occurrences. The success rates were calculated over the 1998–2010 (Figure 8e) and 2003–2016 (Figure 8f) time frames, for SeaWiFS and MODIS, respectively. Although both products exhibited peaks in PAR anomalies of different intensities, on the common period of 2003 to 2010, they both agreed on the ability to predict bloom (2004, 2006, and 2008) and nonbloom (2003, 2005, 2007, and 2010) years, with both being unable to predict the 2009 bloom (Figures 8e and 8f). Positive anomalies were also found during the bloom years of 2000, 2002, 2011, 2012, 2013, and 2014, with negative anomalies prevailing during the nonbloom periods of 2001.

4.6. Upwelling South of Madagascar (Lévy et al., 2007; Raj et al., 2010; Srokosz & Quartly, 2013)

Two upwelling indices, based on Chl-a and SST anomalies (Ramanantsoa et al., 2018), were used to investigate possible links between the upwelling south of Madagascar and the phytoplankton bloom. It should be noted that no relationship between the two indices is expected, given the larger spatial area (44–47.5°E; 25–25.8°S) considered for the Chl-based upwelling index. Owing to the very turbulent mesoscale eddy field in the region and the presence of the SICC (mean speed of 9–18 cm/s; Menezes et al., 2014), a lag of 1–4 months between the upwelling and the onset of the bloom would be expected, depending on the mean speed of the current. From the advanced hypotheses, the phytoplankton bloom would occur after a peak in the upwelling intensity, within the 1- to 4-month lag. The Chl-a based upwelling index yielded a 72% success rate at a 2-month lag, with a bloom (nonbloom) occurring when intensity is below (above) the 0 mg/m threshold. The years of 1999, 2000, 2002, 2004, 2006, 2008, 2009, 2012, 2013, and 2014 were correctly hypothesized as bloom years by the aforementioned threshold (Figure 8g). On the other hand, the SST-based upwelling index produced a 63% success rate of bloom/nonbloom occurrence, observed at 1-month lag when the CUI is lower (for bloom) than an optimized threshold of −0.01. The SST-based CUI was at its lowest during the three major blooms (1999, 2006, and 2008; Figure 8h). Importantly, both upwelling indices associate a decrease in coastal upwelling intensity with the presence of the South-East Madagascar Bloom.

4.7. Climate Modes (Raj et al., 2010)

Climate phenomena such as the Indian Ocean Dipole (IOD), Subtropical Indian Ocean Dipole (SIOD), and El Niño–Southern Oscillation (ENSO) will impact the Indian Ocean (Reason et al., 2000; Saji et al., 1999) through oceanic and atmospheric anomalies, and hence exerting a substantial influence on the variability

Table 2
A Summary of the Different Hypotheses Linked to the South-East Madagascar Bloom

Hypothesis	Threshold for bloom occurrence	Lag	Success rate
MLD	<0 m	0	69%
Plankton wave	>0 m^2/s	1 month	68%
Iron/river runoff	>1.66 mm/day	1 month	53%
Ekman pumping	$>0.06 \times 10^{-6}$ m/s	1 month	63%
PAR-SeaWiFS	>0 Einstein·m^{-2}·day^{-1}	0	86%
PAR-MODIS	>0 Einstein·m^{-2}·day^{-1}	0	74%
CUI-Chl	<0 mg/m^3	2 months	74%
CUI-SST	<−0.01	1 month	63%
IOD	>0 °C	1 month	68%
SIOD	>1.08 °C	0	67%
ENSO	<0 °C	1 month	89%

Note. The lag and thresholds for bloom occurrence at which the hypothesis holds, as well as their specific success rate, are stated. MLD = mixed layer depth; PAR = photosynthetically available radiation; SeaWiFS = Sea-viewing Wide Field-of-view Sensor; MODIS = MOderate Resolution Imaging Spectroradiometer; CUI = coastal upwelling index; SST = sea surface temperature; IOD = Indian Ocean Dipole; SIOD = Subtropical Indian Ocean Dipole; ENSO = El Niño–Southern Oscillation.

of biogeochemical processes in the western Indian Ocean (Currie et al., 2013; Dilmahamod et al., 2016; Vinayachandran et al., 2007). The quantitative hypothesis testing yielded a success rate of 68% (67%) for both IOD (SIOD), with a 1-month (0-month) lag and an optimized threshold of 0 (1.08; Figures 9a and 9b). The major bloom years of 1999, 2006, and 2008 were correctly hypothesized as bloom year occurrence. Interestingly, the Niño 3.4 index yielded an 89% success rate at 1-month lag, with a threshold of less than 0 °C for bloom occurrence, corresponding to La Niña events (Figure 9c). Seven out of eight nonbloom years occurred during a Niño 3.4 index above the optimized threshold of 0 °C, whereas 10 out of the 11 bloom years occur during a Niño 3.4 index lower than 0 °C (weak and strong La Niña). Over the entire time series of 19 years, Niño 3.4 index missed only the 2001 and 2002 events. Two of the three major bloom years, namely 1999 and 2008 coincided with strong La Niña events. It should be noted that the variability, in terms of intensity and latitudinal band, of the SICC and its possible influence on the South-East Madagascar Bloom has been tested (not shown here) but no conclusive results were found. A summary of the outputs from the quantitative hypothesis testing is provided in Table 2. The second column indicates the threshold at which bloom occurs, with nonbloom occurrence associated with the opposite (e.g., <0 m for bloom and >0 m for nonbloom occurrences considering the MLD hypothesis).

5. Discussion

The southwest Indian Ocean exhibits an intriguing biological trait, known as the South-East Madagascar Bloom. Occurring in austral summer, the bloom displays substantial temporal and spatial variability. Using a 19-year time series of ocean color satellite data, this paper provides an updated characterization of the bloom. The bloom box used in this study is identical to the one used in Uz (2007) and is appropriate to capture the maximum spatial coverage of the bloom. A new bloom index is defined, based on Uz (2007), by subtracting the Chl-a concentration in a box further offshore from the bloom box. This new index provides a clear and improved diagnosis of the timing and intensity of the South-East Madagascar Bloom. From this bloom index, a minimum Chl-a concentration threshold of 0.07 mg/m^3 was assigned, from which bloom and nonbloom years were identified. Over the 19 years of Chl-a data set, 11 bloom years were identified. Bloom years were further classified as normal or major blooms, with a 0.16-mg/m^3 threshold assigning three major events occurring in 1999, 2006, and 2008. However, no clear evidence of a specific initiation or dissipation month could be perceived, with enhanced Chl-a starting and reaching its climax at distinct months for different bloom years. The bloom is, nonetheless, observed to last approximately 6 weeks and initiates quicker than it dissipates.

Analysis of Argo profiles in high/low Chl-a patches confirmed the development of the bloom within a shallow MLD, as reported by Uz (2007) and Srokosz and Quartly (2013). This is further corroborated by the hypothesis assessment method which concluded a shallowing (deepening) of MLD during bloom (nonbloom) years, at a success rate of 69%. Hence, the hypothesis from Longhurst (2001) can be conclusively rejected. A shallow mixed layer southeast of Madagascar may possibly be associated with vertical stability, allowing phytoplankton density to accumulate at the surface (Niu et al., 2016). The bloom also occurs in waters warmer than 24.8 °C. The ideal temperature range for the nitrogen-fixing cyanobacteria, namely, *Trichodesmium*, was found to be between 24 and 30 °C, in culture studies (Breitbarth et al., 2007). Another condition necessary for nitrogen-fixing blooms is the light availability. The quantitative hypothesis testing showed that the bloom occurred 86% (SeaWiFS) and 74% (MODIS) of the time (over 19-year Chl-a data set) during higher PAR. This confirms the importance of light availability, in agreement with Raj et al. (2010). Accordingly, a thin mixed layer with increased stratification, high-temperature waters, and excess light availability are the right conditions (Capone et al., 1997; Hood et al., 2001, 2004; Subramaniam et al., 2002; Wilson & Qiu, 2008) converging toward the South-East Madagascar Phytoplankton bloom being dominated by nitrogen fixers, as reported by Poulton et al. (2009), Srokosz and Quartly (2013), and Uz (2007). The PHYSAT data analysis also suggest that the region is dominated by the nitrogen-fixing cyanobacteria namely the Synechococcus and Prochlorococcus.

Trace elements/nutrients such as dissolved iron, phosphorous, and silicate may also play an important role in controlling the abundance and distribution of Trichodesmium (Hood et al., 2004). With a general global correspondence between regions of high iron deposition and high N_2-fixation as well as the high iron requirement of the nitrogenase enzyme, it is thought that Trichodesmium growth is limited by availability of iron (Berman-Frank et al., 2001; Hood et al., 2000). However, Wilson and Qiu (2008) stated that the southeast Madagascar region is an area of low dust deposition. Therefore, the idea of the South-East Madagascar Bloom consisting of other organisms apart from nitrogen-fixing ones should not be excluded. It can also be an "echo-bloom" (Boushaba & Pascual, 2005), which is supported from new nitrogen in the euphotic zone, generated from vertically migrating phytoplankton or from nitrogen fixation.

The plankton wave hypothesis proposed by Srokosz et al. (2004), which involves an eastward movement is likely to be associated to the eastward flowing SICC (Palastanga et al., 2007; Siedler et al., 2006). Hence, a plankton wave mechanism is not necessary anymore to explain an eastward propagation. The SICC is modulated by mesoscale eddies (Menezes et al., 2014), and thus, associated eddy diffusivity together with simultaneous plankton growth may play a role in the dispersion of the bloom. Another environmental factor namely wind stress events have been shown to influence phytoplankton blooms in other parts of the ocean (Koné et al., 2009; Yamada et al., 2004; Zhang et al., 2016). Episodic wind events will influence the MLD, hence the stratification, as well as induce positive/negative W_{ek}, impacting the input of nutrients into the euphotic zone. This could potentially play a role for other phytoplankton groups to bloom in the region. For the influence of W_{ek}, the quantitative hypothesis testing correctly predicted the bloom and nonbloom occurrences at 63% with a 1-month lag. The highly significant 2004 positive W_{ek} was observed ~2 months prior to the peak of the bloom during the passage of tropical cyclone Gafilo, over the bloom region. Related intense winds would induce stirring, resulting in a deepening of the mixed layer and nutrients input into the surface layers, triggering increased phytoplankton production (Lin et al., 2003; Shi & Wang, 2007; Subrahmanyam et al., 2002). This would then perhaps explain the shape of the 2004 phytoplankton bloom, which seems to be disconnected from the Madagascan coasts.

From testing the different hypotheses, co-occurrence of La Niña and bloom years resulted in the highest success rate at 89%. ENSO predominantly impacts the Indian Ocean south of 10°S, whereas IOD is more influential north of 10°S (Rao & Behera, 2005). ENSO induces wind stress curl anomalies northwest of Australia, generating interannual variations in the SEMC (Yamagami & Tozuka, 2015). Hence, during La Niña (El Niño) events, a stronger (weaker) SEMC is observed, at a 5- to 15-months lag (Palastanga et al., 2007; Yamagami & Tozuka, 2015). With the eastern Madagascan coastline tilted toward the west, the stronger but less stable SEMC may detach from the continental slope and possibly feed into the Madagascar Basin (Ou & de Ruijter, 1986). With the SIDDIES corridor (Dilmahamod et al., 2018) prevailing at the same latitude as the SEMC, the separation of the current from the coasts could also occur through eddy current interactions. The SEMC is known to largely influence the coastal upwelling south of Madagascar (DiMarco et al., 2000; Lutjeharms & Machu, 2000; Machu et al., 2002; Ramanantsoa et al., 2018), and consequently, a detachment of the current further north would imply a reduction in the current-driven upwelling south of Madagascar.

This is in agreement with the quantitative hypothesis testing which indicates a decreased coastal upwelling intensity during bloom years (Figures 8g and 8h) and in contradiction with previous studies (Lévy et al., 2007; Raj et al., 2010; Srokosz & Quartly, 2013), who hypothesized that a more intense upwelling could lead to the South-East Madagascar Bloom.

One compelling thermohaline feature associated with the bloom is its occurrence within a low-salinity surface layer. This low-salinity signature is present on both sides of the salinity front in the bloom box and, hence, provides an indication that low-salinity surface waters are potentially linked to the South-East Madagascar Bloom. A detachment of the SEMC, owing to La Niña events, could bring the low-salinity coastal waters into the bloom region, increasing the stratification. This increased stratification, with a decreased upwelling south of Madagascar tend to support phytoplankton blooms of nitrogen-fixing cyanobacteria. High concentration of silicate into the bloom region through these SEMC waters would also facilitate nitrogen-fixation-supported diatom blooms.

6. Summary and Future Work

The sporadic South-East Madagascar Bloom is a distinctive biological feature occurring in the oligotrophic southwest Indian Ocean. This austral summer bloom displays substantial variability in terms of temporal and spatial extent. Several hypotheses have been suggested to explain the physical-biogeochemical mechanisms triggering this feature, but none has been as yet clearly substantiated. This study aims at giving a new definition to the South-East Madagascar Bloom using long-term remotely sensed ocean color data as well as in situ measurements.

A novel bloom index is proposed, based on the difference of Chl-a concentration between a bloom box and a similarly sized box offshore, so as to distinguish bloom years from nonbloom years. This new index provides a better insight on the timing and intensity of the bloom. The bloom is observed to migrate northward and southward from the mean latitudinal band of 22–32°S, with a mean zonal extent up to 70°E. From a co-located Argo profiles and high/low Chl-a patches analysis, the bloom is observed to occur in a shallow-stratified MLD, with a low-salinity signature in the surface layers. These fresher waters are speculated to arrive from the low-salinity coastal-trapped SEMC waters.

A revisit of the different hypotheses presented in preceding studies is performed through a quantitative hypothesis testing. The main outcome showed that bloom years occurred when Niño 3.4 index was below 0 °C (namely, La Niña events). The southeast Madagascar region undergoes great variability during these events, both on atmospheric and oceanic scales. A stronger SEMC during La Niña should favor a detachment from the coast, weakening the current-driven upwelling south of Madagascar. This separation from the coasts can bring low-salinity coastal waters into the Madagascar Basin, inducing an increase in the stratification and, together with excess light availability, providing the right conditions for nitrogen-fixing cyanobacterial phytoplankton bloom. This possible new characteristic of the SEMC and its implication on the bloom shall be addressed in a future modeling study.

Acknowledgments
All the Argo profiles used in this study are freely available from the ARGO program website (http://argo.ucsd.edu/; http://doi.org/10.17882/42182). ISAS temperature and salinity products were produced and distributed by the French Service National d'Observation Argo at LOPS. For access to the PHYSAT data, please contact Séverine Alvain (http://log.cnrs.fr/Physat-2). Dilmahamod A. F. acknowledged funding from the National Research Foundation (NRF; grants 90270 and 98183), the International Centre for Education, Marine and Atmospheric Sciences over Africa (LMI ICEMASA), and the Institut de Recherche pour le Développement (IRD). The financial assistance of the South African Environmental Observation Network (SAEON) toward this research is also acknowledged. Opinions expressed and conclusions arrived at are those of the author and are not necessarily to be attributed to SAEON.

References

Alvain, S., Moulin, C., Dandonneau, Y., & Bréon, F. (2005). Remote sensing of phytoplankton groups in case 1 waters from global SeaWiFS imagery. *Deep Sea Research Part I: Oceanographic Research Papers*, *52*(11), 1989–2004. https://doi.org/10.1016/j.dsr.2005.06.015

Argo (2000). Argo float data and metadata from Global Data Assemby Centre (Argo GDAC). SEANOE, http://doi.org/10.17882/42182

Backeberg, B. C., Penven, P., & Rouault, M. (2012). Impact of intensified Indian Ocean winds on mesoscale variability in the Agulhas system. *Nature Climate Change*, *2*(8), 608–612. https://doi.org/10.1038/nclimate1587

Berman-Frank, I., Cullen, J. T., Shaked, Y., Sherrell, R. M., & Falkowski, P. G. (2001). Iron availability, cellular iron quotas, and nitrogen fixation in Trichodesmium. *Limnology and Oceanography*, *46*(6), 1249–1260. https://doi.org/10.4319/lo.2001.46.6.1249

Böhme, L., & Send, U. (2005). Objective analyses of hydrographic data for referencing profiling float salinities in highly variable environments. *Deep Sea Research Part II*, *52*(3-4), 651–664. https://doi.org/10.1016/j.dsr2.2004.12.014

Boushaba, K., & Pascual, M. (2005). Dynamics of the "echo" effect in a phytoplankton system with nitrogen fixation. *Bulletin of Mathematical Biology*, *67*(3), 487–507. https://doi.org/10.1016/j.bulm.2004.08.004

Breitbarth, E., Oschlies, A., & LaRoche, J. (2007). Physiological constraints on the global distribution of *Trichodesmium*? effect of temperature on diazotrophy. *Biogeosciences*, *4*(1), 53–61. https://doi.org/10.5194/bg-4-53-2007

Capone, D., Zehr, J., Paerl, H., Bergman, B., & Carpenter, E. (1997). Trichodesmium, a globally significant marine cyanobacterium. *Science*, *276*(MAY), 1221–1229.

Chacko, N. (2017). Chlorophyll bloom in response to tropical cyclone Hudhud in the Bay of Bengal: Bio-Argo subsurface observations. *Deep-Sea Research Part I: Oceanographic Research Papers*, *124*, 66–72. https://doi.org/10.1016/j.dsr.2017.04.010

Chu, P. C., Wang, Q., & Bourke, R. H. (1999). A geometric model for the Beaufort/Chukchi Sea thermohaline structure. *Journal of Atmospheric and Oceanic Technology*, *16*(6), 613–632. https://doi.org/10.1175/1520-0426(1999)016<0613:AGMFTB>2.0.CO;2

Currie, J. C., Lengaigne, M., Vialard, J., Kaplan, D. M., Aumont, O., Naqvi, S. W., & Maury, O. (2013). Indian Ocean Dipole and El Niño/Southern Oscillation impacts on regional chlorophyll anomalies in the Indian Ocean. *Biogeosciences*, *10*(10), 6677–6698. https://doi.org/10.5194/bg-10-6677-2013

Dale, A. W., Nickelsen, L., Scholz, F., Hensen, C., Oschlies, A., & Wallmann, K. (2015). A revised global estimate of dissolved iron fluxes from marine sediments. *Global Biogeochemical Cycles*, *29*, 691–707. https://doi.org/10.1002/2014GB005017

Dee, D. P., Uppala, S. M., Simmons, A. J., Berrisford, P., Poli, P., Kobayashi, S., et al. (2011). The ERA-Interim reanalysis: Configuration and performance of the data assimilation system. *Quarterly Journal of the Royal Meteorological Society*, *137*(656), 553–597. https://doi.org/10.1002/qj.828

DiMarco, S. F., Chapman, P., & Nowlin, J. (2000). Satellite observations of upwelling on the continental shelf south of Madagascar. *Geophysical Research Letters*, *27*(24), 3965–3968. https://doi.org/10.1029/2000GL012012

Dilmahamod, A. F., Aguiar-González, B., Penven, P., Reason, C. J. C., De Ruijter, W. P. M., Malan, N., & Hermes, J. C. (2018). SIDDIES corridor: A major east-west pathway of long-lived surface and subsurface eddies crossing the subtropical South Indian Ocean. *Journal of Geophysical Research: Oceans*, *123*, 5406–5425. https://doi.org/10.1029/2018JC013828

Dilmahamod, A. F., Hermes, J. C., & Reason, C. J. (2016). Chlorophyll-a variability in the Seychelles-Chagos Thermocline Ridge: Analysis of a coupled biophysical model. *Journal of Marine Systems*, *154*, 220–232. https://doi.org/10.1016/j.jmarsys.2015.10.011

Gaillard, F., Reynaud, T., Thierry, V., Kolodziejczyk, N., & Von Schuckmann, K. (2016). In situ-based reanalysis of the global ocean temperature and salinity with ISAS: Variability of the heat content and steric height. *Journal of Climate*, *29*(4), 1305–1323. https://doi.org/10.1175/JCLI-D-15-0028.1

Hood, R. R., Bates, N. R., Capone, D. G., & Olson, D. B. (2001). Modeling the effect of nitrogen fixation on carbon and nitrogen fluxes at BATS. *Deep Sea Research Part II: Topical Studies in Oceanography*, *48*(8-9), 1609–1648. https://doi.org/10.1016/S0967-0645(00)00160-0

Hood, R. R., Coles, V. J., & Capone, D. G. (2004). Modeling the distribution of Trichodesmium and nitrogen fixation in the Atlantic Ocean. *Journal of Geophysical Research*, *109*(C6), C06006. https://doi.org/10.1029/2002JC001753

Hood, R. R., Michaels, A. F., & Capone, D. G. (2000). Answers sought to the enigma of marine nitrogen fixation. *Eos, Transactions American Geophysical Union*, *81*(13), 133. https://doi.org/10.1029/00EO00086

Huhn, F., von Kameke, A., Pérez-Muñuzuri, V., Olascoaga, M. J., & Beron-Vera, F. J. (2012). The impact of advective transport by the South Indian Ocean Countercurrent on the Madagascar plankton bloom. *Geophysical Research Letters*, *39*, L06602. https://doi.org/10.1029/2012GL051246

Jeandel, C., Peucker-Ehrenbrink, B., Jones, M., Pearce, C., Oelkers, E., Godderis, Y., et al. (2011). Ocean margins: The missing term in oceanic element budgets? *EOS Transactions, American Geophysical Union*, *92*(26), 217–224.

Johnson, K. S., Chavez, F. P., & Friederich, G. E. (1999). Continental-shelf sediment as a primary source of iron for coastal phytoplankton. *Nature*, *398*(6729), 697–700. https://doi.org/10.1038/19511

Kolodziejczyk, N., Prigent-Mazella, A., & Gaillard, F. (2017). ISAS-15 temperature and salinity gridded fields. SEANOE, http://doi.org/10.17882/52367

Koné, V., Aumont, O., Lévy, M., & Resplandy, L. (2009). Physical and biogeochemical controls of the phytoplankton seasonal cycle in the Indian Ocean: A modeling study. *Geophysical Monograph Series*, *185*, 147–166. https://doi.org/10.1029/2008GM000700

Lavender, S., Jackson, T., & Sathyendranath, S. (2015). The ocean colour climate change initiative: Merging ocean colour observations seamlessly. *Ocean Challenge*, *21*(1), 29–31.

Lévy, M., Ferrari, R., Franks, P. J., Martin, A. P., & Rivière, P. (2012). Bringing physics to life at the submesoscale. *Geophysical Research Letters*, *39*, L14602. https://doi.org/10.1029/2012GL052756

Lévy, M., Shankar, D., André, J. M., Shenoi, S. S., Durand, F., & de Boyer Montégut, C. (2007). Basin-wide seasonal evolution of the Indian Ocean's phytoplankton blooms. *Journal of Geophysical Research*, *112*, C12014. https://doi.org/10.1029/2007JC004090

Li, H., Liu, Z., Xu, J., Wu, X., Sun, C., Lu, S., & Cao, M (2017). Manual of Global Ocean Argo gridded data set (BOA-Argo) (Version, 2017). https://doi.org/10.1002/2016JC012285.6

Li, H., Xu, F., Zhou, W., Wang, D., Wright, J. S., Liu, Z., & Lin, Y. (2017). Development of a global gridded Argo data set with Barnes successive corrections. *Journal of Geophysical Research: Oceans*, *122*, 866–889. https://doi.org/10.1002/2016JC012285

Lin, I., Liu, W. T., Wu, C. C., Wong, G. T., Hu, C., Chen, Z., et al. (2003). New evidence for enhanced ocean primary production triggered by tropical cyclone. *Geophysical Research Letters*, *30*(13), 1718. https://doi.org/10.1029/2003GL017141

Longhurst, A. (2001). A major seasonal phytoplankton bloom in the Madagascar Basin. *Deep-Sea Research Part I: Oceanographic Research Papers*, *48*(11), 2413–2422. https://doi.org/10.1016/S0967-0637(01)00024-3

Lutjeharms, J. R., & Machu, E. (2000). An upwelling cell inshore of the East Madagascar Current. *Deep-Sea Research Part I: Oceanographic Research Papers*, *47*(12), 2405–2411. https://doi.org/10.1016/S0967-0637(00)00026-1

Machu, E., Lutjeharms, J. R. E., Webb, A. M., & Van Aken, H. M. (2002). First hydrographic evidence of the southeast Madagascar upwelling cell. *Geophysical Research Letters*, *29*(21), 2009. https://doi.org/10.1029/2002GL015381

Menezes, V. V., Phillips, H. E., Schiller, A., Bindoff, N. L., Domingues, C. M., & Vianna, M. L. (2014). South Indian countercurrent and associated fronts. *Journal of Geophysical Research: Oceans*, *119*, 6763–6791. https://doi.org/10.1002/2014JC010076

Naik, R. K., George, J. V., Soares, M. A., Devi, A., Anilkumar, N., Roy, R., et al. (2015). Phytoplankton community structure at the juncture of the Agulhas Return Front and Subtropical Front in the Indian Ocean sector of Southern Ocean: Bottom-up and top-down control. *Deep-Sea Research Part II: Topical Studies in Oceanography*, *118*, 233–239. https://doi.org/10.1016/j.dsr2.2015.01.002

Niu, L., van Gelder, P. H., Zhang, C., Guan, Y., & Vrijling, J. K. (2016). Physical control of phytoplankton bloom development in the coastal waters of Jiangsu (China). *Ecological Modelling*, *321*, 75–83. https://doi.org/10.1016/j.ecolmodel.2015.10.008

Ou, H.-W., & de Ruijter, W. P. M. (1986). Separation of an inertial boundary current from a curved coastline. *Journal of Physical Oceanography*, *16*(2), 280–289.

Owens, W. B., & Wong, A. P. (2009). An improved calibration method for the drift of the conductivity sensor on autonomous CTD profiling floats by θ–S climatology. *Deep Sea Research Part I*, *56*(3), 450–457. https://doi.org/10.1016/j.dsr.2008.09.008

Palastanga, V., van Leeuwen, P. J., Schouten, M. W., & de Ruijter, W. P. M. (2007). Flow structure and variability in the subtropical Indian Ocean: Instability of the South Indian Ocean Countercurrent. *Journal of Geophysical Research*, *112*, C01001. https://doi.org/10.1029/2005JC003395

Poulton, A. J., Stinchcombe, M. C., & Quartly, G. D. (2009). High numbers of Trichodesmium and diazotrophic diatoms in the southwest Indian Ocean. *Geophysical Research Letters*, *36*, L15610. https://doi.org/10.1029/2009GL039719

Raj, R. P., Peter, B. N., & Pushpadas, D. (2010). Oceanic and atmospheric influences on the variability of phytoplankton bloom in the Southwestern Indian Ocean. *Journal of Marine Systems*, *82*(4), 217–229. https://doi.org/10.1016/j.jmarsys.2010.05.009

Ramanantsoa, J. D., Krug, M., Penven, P., Rouault, M., & Gula, J. (2018). Coastal upwelling south of Madagascar: Temporal and spatial variability. *Journal of Marine Systems*, *178*(October 2017), 29–37. https://doi.org/10.1016/j.jmarsys.2017.10.005

Rao, S. A., & Behera, S. K. (2005). Subsurface influence on SST in the tropical Indian Ocean: structure and interannual variability. *Dynamics of Atmospheres and Oceans*, *39*(1-2), 103–135. https://doi.org/10.1016/j.dynatmoce.2004.10.014

Reason, C., Allan, R., Lindesay, J., & Ansell, T. (2000). ENSO and climatic signals across the Indian Ocean Basin in the global context: part I, interannual composite patterns. *International Journal of Climatology*, *20*(11), 1285–1327. https://doi.org/10.1002/1097-0088(200009)20:11<1285::AID-JOC536>3.0.CO;2-R

Saji, N. H., Goswami, B. N., Vinayachandran, P. N., & Yamagata, T. (1999). A dipole mode in the tropical Indian Ocean. *Nature*, *401*(6751), 360–3. https://doi.org/10.1038/43854

Sallée, J. B., Speer, K., Morrow, R., & Lumpkin, R. (2008). An estimate of Lagrangian eddy statistics and diffusion in the mixed layer of the Southern Ocean. *Journal of Marine Research*, *66*(4), 441–463. https://doi.org/10.1357/002224008787157458

Satyendranath, S., Brewin, R., Brockmann, C., Brotas, V., Ciavatta, S., Chuprin, A., et al. (2016). Creating an ocean-colour time series for use in climate studies: The experience of the ocean-colour climate change initiative. Remote Sensing of Environment.

Shi, W., & Wang, M. (2007). Observations of a Hurricane Katrina-induced phytoplankton bloom in the Gulf of Mexico. *Geophysical Research Letters*, *34*, L11607. https://doi.org/10.1029/2007GL029724

Siedler, G., Rouault, M., & Lutjeharms, J. R. (2006). Structure and origin of the subtropical South Indian Ocean Countercurrent. *Geophysical Research Letters*, *33*, L24609. https://doi.org/10.1029/2006GL027399

Srokosz, M. A., & Quartly, G. D. (2013). The Madagascar Bloom: A serendipitous study. *Journal of Geophysical Research: Oceans*, *118*, 14–25. https://doi.org/10.1029/2012JC008339

Srokosz, M. A., Quartly, G. D., & Buck, J. J. H. (2004). A possible plankton wave in the Indian Ocean. *Geophysical Research Letters*, *31*, L13301. https://doi.org/10.1029/2004GL019738

Srokosz, M. A., Robinson, J., McGrain, H., Popova, E. E., & Yool, A. (2015). Could the Madagascar Bloom be fertilized by Madagascan iron? *Journal of Geophysical Research: Oceans*, *120*, 5790–5803. https://doi.org/10.1002/2015JC011075

Subrahmanyam, B., Rao, K. H., Srinivasa Rao, N., Murty, V. S. N., & Sharp, R. J. (2002). Influence of a tropical cyclone on Chlorophyll-a Concentration in the Arabian Sea. *Geophysical Research Letters*, *29*(22), 2065. https://doi.org/10.1029/2002GL015892

Subramaniam, A., Brown, C. W., Hood, R. R., Carpenter, E. J., & Capone, D. G. (2002). Detecting Trichodesmium blooms in SeaWiFS imagery. *Deep Sea Research Part II: Topical Studies in Oceanography*, *49*(1-3), 107–121.

Tett, P. (1987). The ecophysiology of exceptional blooms. *Rapports et Proces-verbaux des Reunions. Conseil International pour l'Exploration de la Mer*, *187*, 47–60.

Uz, B. M. (2007). What causes the sporadic phytoplankton bloom southeast of Madagascar? *Journal of Geophysical Research*, *112*, C09010. https://doi.org/10.1029/2006JC003685

Vinayachandran, P. N., Kurian, J., & Neema, C. P. (2007). Indian Ocean response to anomalous conditions in 2006. *Geophysical Research Letters*, *34*, L15602. https://doi.org/10.1029/2007GL030194

Wilson, C., & Qiu, X. (2008). Global distribution of summer chlorophyll blooms in the oligotrophic gyres. *Progress in Oceanography*, *78*(2), 107–134. https://doi.org/10.1016/j.pocean.2008.05.002

Wong, A. P., Johnson, G. C., & Owens, W. B. (2003). Delayed-mode calibration of autonomous CTD profiling float salinity data by χ-S climatology. *Journal of Atmospheric and Oceanic Technology*, *20*(2), 308–318. https://doi.org/10.1175/1520-0426(2003)020<0308:DMCOAC>2.0.CO;2

Xie, P., & Arkin, P. A. (1997). Global precipitation: A 17-year monthly analysis based on gauge observations, satellite estimates, and numerical model outputs. *Bulletin of the American Meteorological Society*, *78*(11), 2539–2558. https://doi.org/10.1175/1520-0477(1997)078<2539:GPAYMA>2.0.CO;2

Yamada, K., Ishizaka, J., Yoo, S., Kim, H.-c., & Chiba, S. (2004). Seasonal and interannual variability of sea surface chlorophyll a concentration in the Japan/East Sea (JES). *Progress in Oceanography*, *61*(December), 193–211. https://doi.org/10.1016/j.pocean.2004.06.001

Yamagami, Y., & Tozuka, T. (2015). Interannual variability of South Equatorial Current bifurcation and western boundary currents along the Madagascar coast. *Journal of Geophysical Research: Oceans*, *120*, 8551–8570. https://doi.org/10.1002/2015JC011069

Zhang, Z., Lowe, R., Ivey, G., Xu, J., & Falter, J. (2016). The combined effect of transient wind-driven upwelling and eddies on vertical nutrient fluxes and phytoplankton dynamics along Ningaloo Reef, Western Australia. *Journal of Geophysical Research: Oceans*, *121*, 4994–5016. https://doi.org/10.1002/2016JC011791